The Astrophysical Journal Supplement Series, 278:22 (15pp), 2025 May https://doi.org/10.3847/1538-4365/adc679

Impact of Interacting Parameters on Dark Matter in an Interacting Dark Energy Model

Himanshu Chaudhary[1], Ritika Nagpal[2], S. K. J. Pacif[3,4], and G. Mustafa[5,6]
[1] Department of Physics, Babeș-Bolyai University, Kogălniceanu Street, Cluj-Napoca, 400084, Romania; himanshu.chaudhary@ubbcluj.ro, himanshuch1729@gmail.com
[2] Department of Mathematics, Vivekananda College, University of Delhi, New Delhi, India; ritikanagpal.math@gmail.com
[3] Pacif Institute of Cosmology and Selfology (PICS), Sagara, Sambalpur 768224, Odisha, India; shibesh.math@gmail.com
[4] Research Center of Astrophysics and Cosmology, Khazar University, Baku, AZ1096, 41 Mehseti Street, Azerbaijan
[5] Department of Physics, Zhejiang Normal University, Jinhua 321004, People's Republic of China; gmustafa3828@gmail.com
[6] Zhejiang Institute of Photoelectronics and Zhejiang Institute for Advanced Light Source, Zhejiang Normal University, Jinhua, Zhejiang 321004, People's Republic of China
Received 2025 January 30; revised 2025 March 24; accepted 2025 March 25; published 2025 May 2

Abstract

This paper investigates a dark energy model within the Friedmann–Lemaître–Robertson–Walker cosmological framework, considering both interacting and noninteracting scenarios. Introducing an interaction scheme between dark energy and dark matter through a specific ansatz for the dark energy density (ρ_{de}), we derive the Hubble parameter $H(z)$ for both cases. To examine the influence of the interaction parameter on dark matter, we use a combination of observational data sets, including cosmic chronometers, Type Ia supernovae, and baryon acoustic oscillation measurements from the Dark Energy Spectroscopic Instrument Year 1 and Sloan Digital Sky Survey IV. We estimate the posterior distribution of each model parameter using the Markov Chain Monte Carlo method. In our analysis, we treat r_d as a free parameter, allowing late-time data sets to constrain each model's parameters, including H_0, r_d, and $\mathcal{M}$. Our analysis shows that the interaction parameter affects dark matter. Additionally, we plot $H(z)$, $\mu(z)$, $\Delta H(z)$, and $\Delta\mu(z)$ with cosmographic parameters to examine the behavior of the late-time expansion of the Universe. Further, the $Om(z)$ diagnostic is applied to distinguish interacting and noninteracting scenarios from the standard ΛCDM model. Finally, statistical metrics are used to compare different models, evaluate their goodness of fit, and determine the best-fit scenario.

Unified Astronomy Thesaurus concepts: Cosmic microwave background radiation (322)

1. Introduction

The past three decades of research in cosmology have predominantly focused on the concept of late-time acceleration of the Universe as first suggested by observations of Type Ia supernovae (SNe Ia, A. G. Riess et al. 1998; S. Perlmutter et al. 1999). This idea has spurred a plethora of cosmological theories, ranging from the introduction of an additional source of energy in the Universe to modifications of gravity and other innovative ideas aimed at explaining the accelerating expansion of the Universe at late times. Since the initial predictions made in the late 1990s, high-precision observations have increasingly supported this fact, challenging previous notions that attracting gravitational force would lead to a decelerating expansion, and ultimately lead to a big crunch. Among the various frameworks proposed to explain cosmic acceleration, the concept of dark energy (DE) has gained wide acceptance among researchers. In the standard cosmological model, DE is often described as a cosmological constant, characterized by a fixed energy density that remains constant regardless of the evolution of other cosmic components. However, this noninteracting scenario faces significant challenges, particularly concerning the fine-tuning and coincidence problems. These issues raise fundamental questions about the precise balance and timing of DE's influence on cosmic expansion (S. Weinberg 1989; P. J. Steinhardt et al. 1999). To address these challenges, alternative models of DE have been proposed, such as dynamic DE and modified gravity theories, which seek to provide a more nuanced understanding of the interplay between DE and the expansion of the Universe. Despite ongoing debates, the pursuit of a deeper understanding of DE remains a central goal in contemporary cosmological research, driving investigations that could potentially reshape our comprehension of the Universe's fate.

To resolve these issues, interacting dark energy (IDE) models have been proposed, where energy is exchanged between DE and dark matter (DM). These interactions offer a potential explanation for the smooth transition from decelerated to accelerated expansion by correlating the evolution of both components (J.-H. He et al. 2009b). The IDE models also allow for a more natural solution to the coincidence problem by ensuring that DE becomes dominant only at the appropriate cosmic epoch. Additionally, energy exchange may alter the formation and growth of structures in the Universe, which motivates further investigation of these models (R. Nagpal & S. K. J. Pacif 2021; K. R. Mishra et al. 2023; C. Rodriguez-Benites et al. 2024).

A prominent hypothesis for DM and DE interaction suggests that any two distinct fields may interact, whether viewed through the lens of particle physics or at a more theoretical level. Cosmologists are interested in this phenomenological approach due to its potential for a variety of novel predictions. Today, understanding the "dark sector" of the Universe has become a central focus, especially as it relates to interactive models of DM and DE that have been the hot topics in the past few years. Simulations indicate that interacting models could address some of the major challenges faced by the standard ΛCDM model, specifically the coincidence and cosmological constant problems, by allowing DE to decay into DM (L. Amendola 2000; F. Costa et al. 2012). Some researchers addressing the coincidence

problem have proposed a DM–DE relationship under certain reasonable assumptions. While the exact nature of DM and DE remains unknown, field theory does provide a framework for potential interaction between them. Viewing the energy densities of DM and DE as dynamic in this manner helps to alleviate the coincidence problem. Numerous studies have explored the connection between DM and DE interactions, including work by E. Abdalla et al. (2010), S. Micheletti et al. (2009), and V. Salvatelli et al. (2014). For a more comprehensive list of findings on the evidence of DM–DE interactions, as well as discussions of their theoretical and cosmological implications, see G. R. Farrar & P. J. E. Peebles (2004), M. Baldi (2011), R.-G. Cai & A. Wang (2005), E. J. Copeland et al. (2006), A. A. Costa et al. (2014), V. Salvatelli et al. (2013), K. R. Mishra et al. (2023), and J. Singh & R. Nagpal (2024).

The interacting scenario in cosmology considers the potential energy exchange between DE and DM, introducing a dynamic model to understand the accelerated expansion of the Universe. A primary reason for exploring this approach is to address the cosmic coincidence problem, which questions why DM and DE densities are similar in magnitude today, despite their distinct characteristics and evolutionary paths (L. Amendola 2000; J.-H. He et al. 2009a). This model also adds flexibility to cosmic evolution, impacting important parameters such as the Hubble and deceleration parameters, allowing it to describe the shift from deceleration to acceleration in a way that may better match observational data (G. R. Farrar & P. J. E. Peebles 2004). Moreover, by altering the growth rate of matter structures through energy exchange between DM and DE, interacting models offer new perspectives on galaxy and cluster formation, along with other observable cosmic structures (M. Baldi 2011; S. Hussain et al. 2024). In the noninteracting scenario, as outlined in the ΛCDM model, DM and DE are considered to evolve independently, with DE acting as a constant cosmological term. ΛCDM's mathematical simplicity and predictive accuracy have made it the foundation of modern cosmology, as it closely aligns with observational data from supernovae, cosmic microwave background (CMB) measurements, and large-scale galaxy surveys (A. A. Penzias & R. W. Wilson 1965; J. Huchra et al. 1983; B. Maffei et al. 2022; C. S. Saraf & P. Bielewicz 2024). Although limitations such as the fine-tuning problem persist, the noninteracting scenario remains effective in explaining the large-scale structure of the Universe. It serves as a crucial benchmark for evaluating alternative models, including those involving DM–DE interactions. Deviations from expected trends in noninteracting models, such as discrepancies in the growth rate of matter structures or anomalies in the rate of cosmic expansion, suggest areas where more complex models could potentially offer deeper insights (R. C. Nunes & S. Vagnozzi 2021; N. Nazari Pooya 2024). Thus, while the noninteracting scenario provides a robust framework for explaining cosmic acceleration, it also highlights opportunities for future advancements in cosmological modeling.

The learning–interaction theory offers the advantage of allowing the DE equation of state (EOS) parameter to shift from quintessence to phantom, effectively yielding a quintom-like behavior in the DE EOS. Furthermore, interaction theory has shown particular efficacy in addressing the discrepancy in the Hubble constant values (H_0) between global and local measurements, providing a promising framework for resolving this long-standing tension (A. G. Riess et al. 2019; L. Verde et al. 2019; K. C. Wong et al. 2020; E. Di Valentino et al. 2021).

The literature presents a range of linear and nonlinear interaction functions, with flexibility to propose new ones, as no universal criterion exists for their selection. Although studies utilizing nonlinear interaction functions (F. Arevalo et al. 2012) are less common, exploring the dynamics of the Universe through nonlinear models remains an intriguing approach. Motivated by the above discussions, we adopt a model-independent approach in this analysis to evaluate an interacting model, aiming to uncover potential new insights, particularly in the late-time-accelerating scenario. (Y. L. Bolotin et al. 2015; W. Yang et al. 2016).

This study focuses on comparing the interacting and noninteracting scenarios of DE and DM within a spatially flat Friedmann–Lemaître–Robertson–Walker (FLRW) universe. We investigate the evolution of key cosmological parameters, including the Hubble parameter, deceleration parameter, and EOS, under both frameworks to assess their influence on cosmic acceleration. Observational data from cosmic chronometers (CCs), SNe Ia, and baryon acoustic oscillations (BAOs) will be use to constrain the model parameters. This comparative approach aims to determine whether interactions between DM and DE offer a more coherent explanation for cosmic evolution and large-scale structure dynamics. The structure of this paper is arranged as follows: Section 1 provides a basic overview of general relativity (GR) and the most pressing cosmological issues. Section 2 outlines the fundamental setup of the governing equations describing matter–energy interactions within GR, including an examination of the spacetime metric and the formulation of the Einstein field equations (EFEs). In Section 3, we discuss the mathematical framework for interacting cosmologies. Section 4 establishes the foundation and motivation for solving the field equations. Section 5 presents two models interacting and noninteracting scenarios which are then constrained using cosmological data. Section 6 describes the methodology and data, along with the Markov Chain Monte Carlo (MCMC) results. Sections 7 and 8 focus on cosmographic analysis and diagnostic profile respectively. Section 9 introduces the statistical metrics. Finally, Section 10 discusses the results and outcomes of the study, and Section 11 summarizes the conclusions.

2. Field Equations with Cosmic Matter–Energy Interactions

We start with the FLRW metric, which characterizes a spatially homogeneous and isotropic universe, elegantly framed within a spherically symmetric geometric structure,

$$ds^2 = -dt^2 + a(t)^2[dr^2 + r^2(d\theta^2 + \sin^2\theta d\phi^2)]. \quad (1)$$

As a function of cosmic time t, the function $a(t)$ represents the scale factor of the Universe in this context. As recent data emphasizes on the flat geometry of the Universe, in this analysis we focus on the flat geometry only.

For the spherically symmetric FRW metric in GR, the EFEs are expressed as

$$R_{\mu\nu} - \frac{1}{2}Rg_{\mu\nu} = 8\pi G T_{\mu\nu}, \quad (2)$$

where $R_{\mu\nu}$ is the Ricci tensor, R is the Ricci scalar, and $T_{\mu\nu}$ denotes the energy–momentum tensor. The left-hand side encapsulates the curvature of spacetime, while the right-hand side represents the energy–matter content, including contributions

from radiation, baryonic matter, DM, and DE. The EFEs, reformulated in terms of physical and geometrical parameters at background order, become

$$\left(\frac{\dot{a}}{a}\right)^2 = \frac{8\pi G}{3}(\rho_r + \rho_b + \rho_{\rm dm} + \rho_{\rm de}) = \frac{8\pi G}{3}\rho_{\rm tot}. \quad (3)$$

Here, ρ_r represents the energy density of radiation, ρ_b that of baryonic matter, $\rho_{\rm dm}$ corresponds to DM energy density, and $\rho_{\rm de}$ denotes DE density. The total energy density is given by $\rho_{\rm tot}$. The equation governing the acceleration of the Universe's expansion is

$$2\frac{\ddot{a}}{a} + \left(\frac{\dot{a}}{a}\right)^2 = -8\pi G(p_r + p_b + p_{\rm dm} + p_{\rm de}) = -8\pi G p_{\rm tot}, \quad (4)$$

where p_r, p_b, $p_{\rm dm}$, and $p_{\rm de}$ are the pressures associated with radiation, baryonic matter, DM, and DE, respectively. The total pressure is denoted by $p_{\rm tot}$. These equations provide a comprehensive framework for describing the evolution of the Universe, encapsulating the dynamic interplay between geometry and the energy–matter components over cosmic time.

In this paper, the time derivative is represented by an overhead dot, and the Hubble parameter is defined as

$$H = \frac{\dot{a}}{a}. \quad (5)$$

Next, we will discuss the continuity equation from the Bianchi identity. The Bianchi identity states that the covariant divergence of the Einstein tensor is zero, expressed as

$$G^{;\nu}_{\mu\nu} = 0. \quad (6)$$

As a result, the energy–momentum tensor also satisfies the conservation equation

$$T^{;\nu}_{\mu\nu} = 0. \quad (7)$$

This equation reflects the conservation of energy and momentum in the Universe. The continuity equation derived from this conservation law plays a crucial role in modeling the evolution of energy densities and pressures for radiation, baryons, DM, and DE.

$$\dot{\rho}_{\rm tot} + 3\frac{\dot{a}}{a}(\rho_{\rm tot} + p_{\rm tot}) = 0. \quad (8)$$

3. Mathematical Framework for Interacting Cosmological Models

In current cosmology, the accelerated expansion of the Universe is assumed to be driven by DE, a component with highly negative pressure. However, treating DM and DE as independent entities may oversimplify the cosmic dynamics. Recent research suggests that allowing interactions between these two components can provide new insights and address key challenges, such as the observed discrepancies in the Hubble parameter between early- and late-time measurements.

In this article, we shift our focus to the interacting scenario, expanding on the motivation outlined in the introduction and earlier discussions. In interacting models, energy and momentum are exchanged between these dark sectors, affecting their densities and the Universe's expansion too. The following equations emerge under the assumption that DM and DE are the two most significant components driving gravitational interactions:

$$\dot{\rho}_r + 3\frac{\dot{a}}{a}(\rho_r + p_r) = 0, \quad (9)$$

$$\dot{\rho}_b + 3\frac{\dot{a}}{a}(\rho_b + p_b) = 0, \quad (10)$$

$$\dot{\rho}_{\rm dm} + 3\frac{\dot{a}}{a}(\rho_{\rm dm} + p_{\rm dm}) = Q(t), \quad (11)$$

and

$$\dot{\rho}_{\rm de} + 3\frac{\dot{a}}{a}(\rho_{\rm de} + p_{\rm de}) = -Q(t). \quad (12)$$

The interaction parameter $Q(t)$ quantifies the strength and direction of the energy transfer between DM and DE, appearing in the modified conservation equations above (Equations (11) and (12)). The sign of Q determines the energy transfer direction:

$Q > 0$: energy flows from DE to DM.

$Q < 0$: energy flows from DM to DE (W. Zimdahl 2012; B. Wang et al. 2016; K. J. Ludwick & H. Sebaugh 2021; A. Aich 2023; Ashmita et al. 2024). However, the exact nature of this interaction remains uncertain. To investigate dark-sector interactions, it is necessary to assume specific plausible forms for Q. In this article, we explore such forms and their implications.

These models also offer a way to resolve some cosmological tensions and influence the formation of large-scale structures, providing a framework to reconcile theoretical predictions with observational data (L. Amendola 2000; E. Majerotto et al. 2009; B. Wang et al. 2016; W. Yang et al. 2018). Also, from thermodynamic perspective, the interaction modifies the entropy production and energy distribution within the cosmic fluid. Energy exchange between DM and DE influences the thermal history of the Universe. If $Q > 0$, DE decays into DM, sustaining cosmic acceleration and slowing the loss of DE. Conversely, if $Q < 0$, energy transfer from DM to DE accelerates the expansion but reduces the available DM, potentially affecting structure formation. The exact nature and implications of the energy flow depend critically on the underlying model of DE, which remains a subject of intense debate. For example: If DE is represented by the cosmological constant (Λ), interaction scenarios must respect the constant nature of vacuum energy density, leading to distinct constraints on the form of Q. If DE arises from a dynamic scalar field (e.g., quintessence or k-essence), the interaction introduces additional complexities, as the scalar field evolves with time and potentially couples to DM in diverse ways. The uncertainty surrounding the true nature of DE makes it challenging to precisely determine the energy exchange mechanism and its impact. Different DE candidates lead to different predictions for the flow of energy between the sectors, highlighting the need for further theoretical and observational exploration to constrain these interactions.

3.1. Theoretical Basis and Selection of Interaction Terms in DE and DM

To understand the coupling dynamics between DM and DE, the choice of an appropriate interaction term Q is crucial. Since the precise nature of this interaction remains unknown,

researchers typically assume specific functional forms for Q that align with cosmological principles and are consistent with observational data. This approach provides a framework to explore the possible impacts of DM–DE interactions on cosmic evolution.

A commonly adopted class of interaction terms leverages the Hubble parameter H and the energy densities of DM and DE (M. B. Gavela et al. 2010; B. Wang et al. 2016; W. Yang et al. 2018). Two widely studied forms for the interaction term include

$$Q = \xi H \rho_{\rm dm} \quad \text{and} \quad Q = \xi H (\rho_{\rm dm} + \rho_{\rm de}),$$

where ξ is a dimensionless coupling constant that controls the strength of the interaction between DM and DE. In these forms, Q is directly proportional to the Hubble parameter H, thereby ensuring that the interaction term dynamically scales with the expansion of the Universe. The first expression, $Q = \xi H \rho_{\rm dm}$, models the interaction based solely on the DM energy density, while the second form, $Q = \xi H (\rho_{\rm dm} + \rho_{\rm de})$, considers contributions from both DM and DE energy densities.

These formulations provide a flexible basis for investigating different coupling strengths and their influence on the behavior of DM and DE over cosmic time, contributing to our understanding of potential deviations from the standard ΛCDM model.

3.2. Hubble-dependent Interaction Term Selection

The interaction term is frequently modeled to be proportional to the Hubble parameter and the energy densities for several reasons:

1. *Dependence on Cosmic Expansion.* The Hubble parameter H, representing the Universe's expansion rate, is a natural choice for modeling DM–DE interactions, allowing the interaction to dynamically evolve with cosmic expansion (C. Wetterich 1995; L. Amendola 2000).
2. *Smooth Evolution across Epochs.* An interaction term proportional to H enables smooth energy transfer across the radiation, matter, and dark-energy-dominated phases, ensuring seamless cosmic evolution (K. Bamba et al. 2012).
3. *Consistency with Observations.* The forms $Q = \xi H \rho_{\rm dm}$ or $Q = \xi H (\rho_{\rm dm} + \rho_{\rm de})$ align well with current cosmological observations, including CMB measurements, supernovae data, and the formation of large-scale structures. These forms balance simplicity with empirical accuracy, allowing meaningful comparisons with observations (E. Komatsu et al. 2011; Y. Liu et al. 2022).
4. *Mitigating Fine-tuning Issues.* As noted in Section 1, interacting models alleviate the fine-tuning problem. Simple forms involving H and energy densities reduce parameter tuning, simplifying both analytical and numerical analysis of the interaction models (G. R. Farrar & P. J. E. Peebles 2004; G. Caldera-Cabral et al. 2009).

In this study we have chosen the choice of Q as

$$Q = 3\gamma H \rho_{\rm dm}, \tag{13}$$

because the interaction term must be proportional to the inverse unit of time (L. Amendola et al. 2007; Z.-K. Guo et al. 2007; D. Pavón & B. Wang 2009) and to hold the continuity law in Equation (8). The coupling constant ξ given in Equation (13) is considered as $\xi = 3\gamma$.

4. Interacting Solutions

For the interacting scenario, the continuity equation (8) can be decomposed into the following individual equations as mentioned in Equations (9), (10), (11), and (12). Equations (9) and (10) can easily be solved to yield

$$\rho_r = \frac{C_1}{a^4}, \tag{14}$$

$$\rho_b = \frac{C_2}{a^3}. \tag{15}$$

We now consider the interaction term in the form $Q = 3\gamma H \rho_{\rm dm}$ as considered in Equation (13). By solving Equations (11) and (12) for the this specific choice of $Q(t)$, we obtain the following result:

$$\rho_{\rm dm} = \frac{C_3}{a^{3(1-\gamma)}}, \tag{16}$$

and

$$\dot{\rho}_{\rm de} + 3\frac{\dot{a}}{a}(1 + \omega_{\rm de})\rho_{\rm de} = -3H\gamma C_3 a^{3(\gamma-1)}, \tag{17}$$

where C_1, C_2, and C_3 are integrating constants.

The EOS for various energy components in the Universe is represented as $w_i = \frac{P_i}{\rho_i}$; i stands for radiation (r), matter (m), and DE (de). Since, the dust matter pressure is zero and in the late Universe the contribution of radiation is negligible, one can suggest $p_m = 0$ and $p_r \approx 0$. The EOS of DE would be $w_{\rm de} = \frac{p_{\rm de}}{\rho_{\rm de}}$, which will be a function of scale factor (a) or redshift (z), where the redshift is defined as $1 + z = \frac{a_0}{a}$. And for simplification, we adopt here the standard convention of normalizing the present-day scale factor to $a_0 = 1$.

The solution is then derived from the field equations with explicit forms of expressions of cosmological parameters. Equations (14), (15), and (16) will take the following forms:

$$\rho_r = C_1(1 + z)^4,\ \rho_b = C_2(1 + z)^3,$$
$$\rho_{\rm dm} = C_3(1 + z)^{3(1-\gamma)}. \tag{18}$$

To solve the equations of motion, an additional equation is required for a deterministic solution. One of the simplest approaches is to use a model-independent way, such as cosmological parameterization. Since physical and geometrical parameters vary as functions of the independent variable, either time t or redshift z, it is convenient to parameterize any relevant parameter to achieve a deterministic solution without violating the underlying theoretical framework.

In recent years, various researchers have utilized this approach, proposing different parameterizations for the energy density of DE to model its dynamic behavior and assess its impact on the Universe's expansion. These parameterizations provide a means to describe potential deviations from the standard ΛCDM model, in which the energy density of DE remains constant. By exploring different functional forms, cosmologists aim to gain insights into cosmic acceleration, address observational discrepancies, and predict the Universe's future evolution. Some well-known density parameterizations are as follows:

1. *Constant Density Parameterization (ΛCDM Model).*

$$\rho_{\rm de} = \text{constant}. \tag{19}$$

This corresponds to the cosmological constant but faces challenges like the fine-tuning problem (B. Wang et al. 2016).

2. *Linear Parameterizations*. The linearly varying DE density form

$$\rho_{\rm de}(z) = \rho_{\rm de_0}(1 + \beta \cdot z), \tag{20}$$

and exponential models introduce slow variations, aiding in the study of intermediate redshift deviations (L. Amendola 2000).

3. *Power-law Parameterization.* The power-law-varying DE density is represented as (G. Montani et al. 2025)

$$\rho_{\rm de} \propto a^{-n}, \tag{21}$$

4. *Interaction-based Parameterization.* This parameterization evolves with redshift z as

$$\rho_{\rm de}(z) = \beta\left(1 + \alpha\left(\frac{z}{1+z}\right)^n\right), \tag{22}$$

where α, n, and $\beta \neq 0$ are model parameters. These models provide additional freedom, helping address the Hubble tension and influencing cosmic structure formation (D. Wang & X.-H. Meng 2017).

4.1. Role of the Model Parameters n, α, and β

In this work, we consider the interaction-based parameterization of the DE density given in Equation (22). In the parameterization considered in Equation (22), one can easily infer that the standard ΛCDM model can be retrieved for $\alpha = 0 \rho_{\rm de}(z) =$ constant. The parameter α, when nonzero, governs the deviation of the DE density from the constant ΛCDM model, allowing for its dynamical evolution. The parameter α governs the evolution strength of DE density with redshift. Higher α values induce greater variations, introducing dynamics that deviate from the constant density of the ΛCDM model. In interacting models, α affects the efficiency of energy transfer between DM and DE, impacting the Hubble and deceleration parameters. Thus, α aids in addressing observational tensions, such as the Hubble constant discrepancy, by modulating cosmic acceleration in line with observational constraints. Moreover, $\beta = 1$ is the case of a dynamical DE density model and $\beta \neq 1$ acts as a scaling factor, modifying the overall magnitude of the energy density. The parameter n in the chosen parameterization dictates the evolution rate of DE density with cosmic expansion. Higher n values lead to faster changes in energy density with redshift, crucial for shaping the Universe's late-time behavior and determining whether DE dominance occurs smoothly or abruptly. In interacting models, n influences the impact of energy exchange on DM clustering and large-scale structure formation. It also plays a key role in predicting outcomes like a potential "Big Rip" or an asymptotic stabilization of the Universe.

Now, with this setup, we can find the mathematical expressions of the physical parameters of the model containing these discussed model parameters n, α, and β. In order to discuss the physical dynamics of the model, we need to calculate $\rho_{\rm de}$ and $p_{\rm de}$. Additionally, we need to calculate $\omega_{\rm de}$. With the help of Equations (16), (17), and (18), we have the following expressions:

$$\rho_{\rm de} = \frac{3}{8\pi G}[H^2] - [C_1(1+z)^4 + C_2(1+z)^3 + C_3(1+z)^{3-3\gamma}], \tag{23}$$

$$p_{\rm de} = \frac{-1}{8\pi G}[(2q-1)H^2] - \frac{1}{3}C_1(1+z)^4, \tag{24}$$

where C_1, C_2, and C_3 represent the contributions from radiation, matter, and a generalized fluid component with parameter γ. The term $(1 + z)$ accounts for the redshift, showing how energy densities evolve with the expansion of the Universe.

Next, we introduce the density parameter Ω_i, which expresses the ratio of an individual energy density ρ_i to the critical density ρ_{cr}. The critical density, necessary for a flat universe, is defined as

$$\rho_{cr} = \frac{3H^2}{8\pi G}. \tag{25}$$

Here, the subscripts $i = r$, b, dm, and de refer to radiation, baryonic matter, DM, and DE, respectively. The density parameter is then given by

$$\Omega_i = \frac{\rho_i}{\rho_{cr}}. \tag{26}$$

This formulation allows us to compare the contributions of different energy components relative to the critical density. The sum of these density parameters Ω_r, Ω_b, $\Omega_{\rm dm}$, and $\Omega_{\rm de}$ provides a complete picture of the Universe's energy content and helps determine whether the Universe is flat, open, or closed.

$$\begin{aligned}
\Omega_r &= \Omega_{\rm rad,0}(1+z)^4\left(\frac{H_0}{H}\right)^2,\\
\Omega_b &= \Omega_{b_0}(1+z)^3\left(\frac{H_0}{H}\right)^2,\\
\Omega_{\rm dm} &= \Omega_{\rm dm_0}(1+z)^{3-3\gamma}\left(\frac{H_0}{H}\right)^2,\\
\Omega_{\rm de} &= 1 - \left(\frac{H_0}{H}\right)^2[\Omega_{\rm rad,0}(1+z)^4 + \Omega_{b_0}(1+z)^3 + \Omega_{\rm dm_0}(1+z)^{3-3\gamma}],
\end{aligned} \tag{27}$$

where the set of equations in (27) represents the different components of the density parameters. Also, Ω_{j_0} denotes the present value of the density parameter of radiation, baryons, DM, and DE at the current moment ($t = t_0$ or $z = 0$) as j takes values r, b, dm, and de respectively.

$$\begin{aligned}
\Omega_{\rm rad,0} &= \frac{C_1\, 8\pi G}{3H_0^2},\ \Omega_{b_0} = \frac{C_2\, 8\pi G}{3H_0^2},\\
\Omega_{\rm dm_0} &= \frac{C_3\, 8\pi G}{3H_0^2},\ \Omega_{\rm de_0} = \frac{\beta\, 8\pi G}{3H_0^2}.
\end{aligned} \tag{28}$$

where the set of equations in (28) represents the present values of the density parameter of these various components.

In terms of the density parameter from Equation (27), our model takes the form as

$$H(z) = H_0(\Omega_{\mathrm{rad},0}(1+z)^4 + \Omega_{b_0}(1+z)^3 + \Omega_{\mathrm{dm}_0}(1+z)^{3(1-\gamma)} + \Omega_{\mathrm{de}_0}\left(1+\alpha\left(\frac{z}{1+z}\right)^n\right)^{\frac{1}{2}}.$$

The deceleration parameter of the Universe can be simply written with the help of the above expression of the Hubble parameter as

$$q(z) = -1 + (1+z)\frac{d\ln H(z)}{dz}. \tag{29}$$

Similarly, the expression for the EOS of DE would be $w_{\mathrm{de}} = \frac{p_{\mathrm{de}}}{\rho_{\mathrm{de}}}$, and this can also be derived from Equations (23), (24), and (27) as a function of redshift (z).

4.2. Interacting Models: Linking Geometric and Interaction Parameters to Cosmic Structure Formation and Hubble Tension

In cosmology, key parameters such as the scale factor $a(t)$, the Hubble parameter $H(t)$, and the deceleration parameter $q(t)$ describe the expansion and acceleration of the Universe over time. In interacting models involving DM and DE, the focus shifts to energy transfer between these components and its impact on cosmic dynamics. In such models, the dark sector functions as a dynamic system with energy flow governed by the interaction parameter γ. The sign of γ determines the direction of energy transfer.

Impact of γ on Cosmic Dynamics. The interaction parameter γ influences both the geometric parameters (e.g., $a(t)$, $H(t)$, $q(t)$) and the energy densities of cosmic components, shaping the Universe's expansion history. This framework enables exploration of dynamics beyond the standard ΛCDM model by modifying cosmic evolution through energy exchange.

The parameters n and α add flexibility to the model, enabling a nuanced approach to cosmic evolution. By modulating the rate and strength of energy transfer between DM and DE, these parameters help address the Hubble tension, that is, the discrepancy in the Hubble constant from early- and late-time observations. They also influence cosmic structure formation by altering DM density growth, impacting galaxy formation and large-scale structures.

These interactions further aid in resolving cosmological tensions by dynamically adjusting energy densities, which modulate the Hubble parameter's evolution over time. This model provides the adaptability needed to explain the growth of large-scale structures and smooth transitions between cosmic epochs. The upcoming section will discuss specific parameter values and offer further insights into the Universe's dynamics under this interaction framework.

5. The Model

Model 1: Interacting Model. The form of $H(z)$ in the case of the interacting scenario is

$$H(z) = H_0\Big[\Omega_{b_0}(1+z)^3 + \Omega_{\mathrm{dm}_0}(1+z)^{3(1-\gamma)} + \Omega_{\mathrm{rad},0}(1+z)^4 + \Omega_{\mathrm{de}_0}\left(1+\alpha\left(\frac{z}{1+z}\right)^n\right)\Big]^{1/2}. \tag{30}$$

Here α, n are model parameters and γ is the interaction-coupling constant.

$\Omega_{\mathrm{rad},0} \rightarrow$ present value of density parameter of radiation.

$\Omega_{m_0} = \Omega_{b_0} + \Omega_{\mathrm{dm}_0} \rightarrow$ present value of the cold DM density (sum of baryonic matter and DM).

$\Omega_{\mathrm{de}_0} \rightarrow$ present value of density parameter of DE.

Model 2: Noninteracting Model. If we consider minimal interaction between the cold DM and the DE, then they conserve separately, which is the case with $\gamma = 0$ here. Then Model 1 reduces to a noninteracting model (Model 2). This means the noninteracting case is a special case of the interacting one. Now, the form of $H(z)$ in the case of the noninteracting scenario is expressed as

$$H(z) = H_0\Big[\Omega_{b_0}(1+z)^3 + \Omega_{\mathrm{dm}_0}(1+z)^3 + \Omega_{\mathrm{rad},0}(1+z)^4 + \Omega_{\mathrm{de}_0}\left(1+\alpha\left(\frac{z}{1+z}\right)^n\right)\Big]^{1/2}. \tag{31}$$

Here α and n are model parameters. Now, we have the models ready to discuss the observational aspects. In the next section, we are going to discuss the data considered here and the methodology we use to constrain the model.

6. Methodology and Data Description

In this study, we utilize the `PyPolyChord` nested-sampling algorithm (W. Handley et al. 2015) to determine the parameter distributions that are consistent with the data for both interacting and noninteracting DE models. The `PyPolyChord` algorithm applies Bayes' theorem to compute the posterior distribution:

$$P(\phi|\mathcal{D}) = \frac{\mathcal{L}(\mathcal{D}|\phi)\pi(\phi)}{\mathcal{Z}},$$

where $P(\phi|\mathcal{D})$ is the posterior probability of the parameters ϕ given the data $\mathcal{D}$, $\mathcal{L}(\mathcal{D}|\phi)$ is the likelihood, $\pi(\phi)$ is the prior, and $\mathcal{Z}$ is the evidence. Unlike traditional MCMC methods that generate a Markov chain to sample from the posterior distribution, `PyPolyChord` uses nested sampling (J. Skilling 2006). This approach iteratively refines a set of live points to efficiently explore the parameter space and manage complex posterior distributions. The likelihood function is defined using a χ^2 measure, which assesses how well the model predictions match the observed data. We choose uniform priors based on existing knowledge, mapping them from the unit hypercube to the parameter space with a custom function. To balance efficiency and accuracy, we use 100 live points. Clustering improves parameter space exploration, and each run begins anew without relying on previous results. A dumping function monitors the progress of live and dead points in real time. In `PyPolyChord` Convergence is achieved when the posterior mass of the live points reaches $p = 10^{-2}$ of the total calculated evidence, ensuring thorough exploration of the parameter space. Outputs include posterior distributions, parameter estimates, and the evidence. We employ the `GetDist` library (A. Lewis 2019), a publicly available toolkit that offers comprehensive functionality for generating 1D and 2D posterior distribution plots.

6.1. Data Description

To determine the parameter distributions, we use the following data sets: CCs, SNe Ia data without SHOES calibration, and BAO data. For the BAO measurements, we include the latest results from Dark Energy Spectroscopic Instrument (DESI) Year 1 and SDSS-IV. Instead of analyzing each data set individually, we consider their combination, as this provides a more robust approach. Analyzing data sets separately can result in degeneracies between correlated parameters. In the following subsections, we briefly describe each data set and the corresponding likelihoods.

6.1.1. Cosmic Chronometers

The concept of CCs was introduced by R. Jimenez & A. Loeb (2002) as a method to measure the Hubble parameter $H(z)$ independently of cosmological models. It relies on the relationship between time t, redshift z, and $H(z)$ in an FLRW universe: $H(z) = -\frac{1}{1+z}\frac{dz}{dt}$. This approach requires precise measurements of redshift dz and differential age evolution dt. While redshift can be measured with high precision through spectroscopy, the challenge lies in determining dt, which necessitates a CC. Massive, early, passively evolving galaxies (e.g., $\log_{10}(M/M_{\odot}) \gtrsim 11$) are ideal candidates as CCs. These galaxies formed their stars rapidly at high redshift ($z \sim 2-3$) and have since evolved passively (A. Cimatti et al. 2004; T. Treu et al. 2005; L. Pozzetti et al. 2010; D. Thomas et al. 2010; J. Choi et al. 2014; M. Onodera et al. 2015; A. Citro et al. 2016; C. Pacifici et al. 2016; A. Carnall et al. 2018; V. Estrada-Carpenter et al. 2018; S. Belli et al. 2019; M. Moresco et al. 2020). The age difference Δt between two such galaxies with a small redshift separation Δz provides an estimate of $dz/dt \approx \Delta z/\Delta t$, enabling the calculation of $H(z)$. Over the last two decades, CC-based $H(z)$ measurements have been extensively studied, providing estimates up to $z \sim 2$ with uncertainties typically around 10% uncertainty (R. Jimenez et al. 2003; J. Simon et al. 2005; D. Stern et al. 2010; M. Moresco et al. 2012; C. Zhang et al. 2014; M. Moresco et al. 2016; A. Ratsimbazafy et al. 2017). In our analysis we consider the latest compilation that includes 31 $H(z)$ measurements in the redshift range $0.07 < z < 1.965$, as summarized in Table 1 of S. Vagnozzi et al. (2021). In the MCMC analysis, we define the $\chi^2_{\rm CC}$ statistic as

$$-2\ln(\mathcal{L}) = \chi^2_{\rm CC} = \Delta \boldsymbol{H}^T(z)\boldsymbol{C}^{-1}\Delta \boldsymbol{H}(z),$$

where $\Delta \boldsymbol{H}(z) = \boldsymbol{H}_{\rm model}(\theta) - \boldsymbol{H}_{\rm obs}$ is the vector of residuals, with $\boldsymbol{H}_{\rm model}(\theta)$ representing the model's theoretical Hubble parameter values at redshifts z_i for the parameter θ, and $\boldsymbol{H}_{\rm obs}$ being the observed Hubble parameter values. Following M. Moresco et al. (2020), the full covariance matrix $\boldsymbol{C}$, which includes both statistical and systematic uncertainties, is considered. Its inverse, $\boldsymbol{C}^{-1}$, is used to incorporate the measurement uncertainties.

6.1.2. Type Ia Supernova

To obtain the distributions consistent with the Pantheon$^+$ data set, which includes light curves for 1701 SNe Ia from 1550 distinct supernovae, spanning a redshift range of $0 \leqslant z \leqslant 2.3$ (D. Brout et al. 2022), we use the widely adopted χ^2 statistic (A. G. Riess et al. 1998; P. Astier et al. 2006), incorporating systematic covariance (A. Conley et al. 2010). The cosmological parameters are constrained by minimizing the χ^2-based likelihood function:

$$-2\ln(\mathcal{L}) = \chi^2_{\rm SNe\ Ia} = \Delta \boldsymbol{D}^T \boldsymbol{C}^{-1}_{\rm total}\,\Delta \boldsymbol{D},$$

where $\Delta \boldsymbol{D}$ is the vector of residuals between the observed distance moduli $\mu(z_i)$ and the model-predicted distance moduli $\mu_{\rm model}(z_i,\ \theta)$. Each element of $\Delta \boldsymbol{D}$, denoted as ΔD_i, is calculated as

$$\Delta D_i = \mu(z_i) - \mu_{\rm model}(z_i, \theta).$$

$\boldsymbol{C}_{\rm total}$ represents the total covariance matrix, which combines both statistical ($\boldsymbol{C}_{\rm stat}$) and systematic ($\boldsymbol{C}_{\rm sys}$) uncertainties in the SNe Ia data. The term $\boldsymbol{C}^{-1}_{\rm total}$ is the inverse of the total covariance matrix. The quantity $\mu_{\rm model}(z_i,\ \theta)$ represents the model-based distance modulus, which depends on the cosmological parameters θ. The model distance moduli are given by

$$\mu_{\rm model}(z_i) = 5\log_{10}\left(\frac{d_{\rm L}(z)}{\rm Mpc}\right) + \mathcal{M} + 25,$$

where, for a flat FLRW universe, the luminosity distance $d_{\rm L}(z)$ is computed using the following expression:

$$d_{\rm L}(z) = c(1+z)\int_0^z \frac{dz'}{H(z')}.$$

Here, c represents the speed of light, and $H(z)$ is the Hubble parameter that describes the expansion history of the Universe. This method highlights the degeneracy between the parameters $\mathcal{M}$ (the absolute magnitude of SNe Ia) and H_0 when analyzing SNe Ia data alone; a crucial consideration in supernova cosmology studies.

6.1.3. Baryon Acoustic Oscillations

We also include the latest BAO data from DESI Year 1 observations (A. Adame et al. 2025), along with data from the completed SDSS-IV extended Baryon Oscillation Spectroscopic Survey (S. Alam et al. 2021). BAO measurements rely on the sound horizon at the epoch of baryon decoupling, r_d, which occurs at $z_d \approx 1060$ in the standard cosmological model. The sound horizon is defined as

$$r_d = \int_{z_d}^{\infty} \frac{c_s(z)}{H(z)}\,dz,$$

The present-day baryon and photon densities, $\rho_{b,0}$ and $\rho_{\gamma,0}$, are given by Planck (Planck Collaboration et al. 2020) values as $\rho_{b,0} = 0.02237\,h^2$ and $\rho_{\gamma,0} = 2.4697 \times 10^{-5}\,h^2$, where $h = H_0/100$. The sound speed, $c_s(z)$, depends on the Hubble parameter $H(z)$. In the flat ΛCDM model, the sound horizon at the drag epoch ($z_d \approx 1060$) is $r_d = 147.09 \pm 0.26$ Mpc (Planck Collaboration et al. 2020). To ensure model independence, r_d is treated as a free parameter in this analysis, allowing constraints on r_d without relying on specific assumptions about recombination-era physics or early Universe conditions (L. Pogosian et al. 2020, 2024 K. Jedamzik et al. 2021; W. Lin et al. 2021; S. Vagnozzi 2023). To obtain the distributions consistent with the BAO data set, we calculate the Hubble distance $D_H(z)$, the comoving angular diameter distance $D_M(z)$, and the volume-

averaged distance $D_V(z)$, defined as follows

$$D_H(z) = \frac{c}{H(z)},$$

$$D_M(z) = c\int_0^z \frac{dz'}{H(z')},$$

$$D_V(z) = [zD_M^2(z)D_H(z)]^{1/3}.$$

To analyze the BAO data set, we consider the following ratios: $\frac{D_M(z)}{r_d}$, $\frac{D_H(z)}{r_d}$, and $\frac{D_V(z)}{r_d}$. The χ^2 statistic for each ratio is given by

$$\chi^2_{D_Y/r_d} = \Delta D_Y^T \cdot \boldsymbol{C}_{D_Y}^{-1} \cdot \Delta D_Y,$$

where $\Delta D_Y = D_{Y/r_d,\text{Model}} - D_{Y/r_d,\text{Data}}$ for $Y = H$, M, V, and $\boldsymbol{C}_{D_Y}^{-1}$ is the inverse of the covariance matrix. The covariance matrix $\boldsymbol{C}_{D_Y}$ is usually diagonal, with elements $\sigma^2_{D_Y}$, representing observational uncertainties, i.e., $\boldsymbol{C}_{D_Y} = \text{diag}(\sigma^2_{D_Y})$. The inverse is $\boldsymbol{C}_{D_Y}^{-1} = (\text{diag}(\sigma^2_{D_Y}))^{-1}$. The total χ^2 is

$$\chi^2_{\text{BAO}} = \chi^2_{D_H/r_d} + \chi^2_{D_V/r_d} + \chi^2_{D_M/r_d}.$$

The total χ^2_{BAO} combines the contributions from the Hubble distance, angular diameter distance, and volume-averaged distance. The distributions of the interacting and noninteracting scenarios are determined by minimizing the chi-square statistic, χ^2, or equivalently, by maximizing the likelihood function, $\mathcal{L}$. The total likelihood, $\mathcal{L}_{\text{tot}}$, relates to the total chi-square, χ^2_{tot}, as $\mathcal{L}_{\text{tot}} \propto e^{-\frac{\chi^2_{\text{tot}}}{2}}$. It is expressed as the product of individual likelihoods:

$$\mathcal{L}_{\text{tot}} = \mathcal{L}_{\text{CC}} \times \mathcal{L}_{\text{SNe Ia}} \times \mathcal{L}_{\text{BAO}},$$

where the total chi-square is

$$\chi^2_{\text{tot}} = \chi^2_{\text{CC}} + \chi^2_{\text{SNe Ia}} + \chi^2_{\text{BAO}}.$$

In our analysis, the interacting model has eight free parameters, while the noninteracting model has seven free parameters along with two derived parameters, Ω_{de_0} and $\Omega_{\text{rad},0}$. The distribution of Ω_{de_0} is extracted using the relation $\Omega_{\text{de}_0} = 1 - \Omega_{\text{dm}_0} - \Omega_{b_0} - \Omega_{\text{rad},0}$, and $\Omega_{\text{rad},0} = (4.183699 \times 10^{-5})\, h^{-2}$, $h = \frac{H_0}{100}$. This approach eliminates the need to explicitly vary Ω_{de_0} and $\Omega_{\text{rad},0}$, as they are fully determined by the other parameters in the model.

6.2. Comparative Analysis with the ΛCDM Model and Observational Data

After obtaining the parameter distributions for the interacting and noninteracting models, our goal is to compare each model with various observational data sets. To achieve this, we will use the mean values and plot the Hubble parameter ($H(z)$), Hubble difference ($\Delta H(z)$), distance modulus ($\mu(z)$), and distance modulus difference ($\Delta\mu(z)$) as functions of redshift for the interacting, noninteracting, and ΛCDM models against the CC and SNe Ia measurements. This approach provides a comprehensive framework for analyzing the interacting and noninteracting models with the standard ΛCDM framework, providing insights into their ability to explain the Universe's late-time expansion and assessing their viability as alternative cosmological models.

6.2.1. Comparison of the ΛCDM Model with Interacting and Noninteracting Models Using the Hubble Parameter H(z) and Hubble Difference ΔH(z)

In this subsection, we compare the interacting and noninteracting models with observational Hubble parameter measurements by plotting $H(z)$ as a function of redshift. The Hubble parameter for the ΛCDM model is given by $H(z) = H_0\sqrt{\Omega_{m0}(1+z)^3 + \Omega_{\Lambda 0}}$. Using the mean values from the MCMC analysis, we calibrate the Hubble parameter for the ΛCDM, interacting, and noninteracting models and compare them with observational data. After plotting the Hubble parameter $H(z)$, we compute and plot the Hubble difference $\Delta H(z)$ as a function of redshift. The difference is given by $\Delta H(z) = H_{\text{model}}(z) - H_{\Lambda\text{CDM}}(z)$, where $H_{\text{model}}(z)$ represents the Hubble parameter for the interacting or noninteracting model, and $H_{\Lambda\text{CDM}}(z)$ represents the Hubble parameter for the standard ΛCDM model. The error bars are obtained using the expression $\Delta H(z_i) = H_{\text{obs}}(z_i) - H_{\Lambda\text{CDM}}(z_i)$, where $H_{\text{obs}}(z_i)$ is the observed Hubble parameter at redshift z_i. The line $\Delta H(z) = 0$ corresponds to the ΛCDM model, providing a baseline for comparison. By calculating $\Delta H(z)$, we can assess how these models deviate from the predictions of the ΛCDM model.

6.2.2. Comparison of the ΛCDM Model with Interacting and Noninteracting Models Using the Distance Modulus μ(z) and Distance Modulus Difference Δμ(z)

In this subsection, we compute the distance modulus, given by $\mu(z) = 5\log_{10}(D_{\text{L}}(z)) + 25$, where $D_{\text{L}}(z)$ is the luminosity distance in Mpc. Using the mean values from the MCMC analysis, we calibrate the distance modulus for the ΛCDM model, the interacting model, and the noninteracting model, denoted as $\mu_{\Lambda\text{CDM}}(z)$, $\mu_{\text{Interacting}}(z)$, and $\mu_{\text{Noninteracting}}(z)$, respectively. To evaluate deviations from the standard ΛCDM model, we compute the residual distance modulus: $\Delta\mu(z) = \mu_{\text{Model}}(z) - \mu_{\Lambda\text{CDM}}(z)$, where $\mu_{\text{Model}}(z)$ represents either the interacting or noninteracting model. This allows us to quantify systematic differences across redshifts. We then compare these predictions with observational data from 1701 SNe Ia. The observational residuals are defined as $\Delta\mu(z_i) = \mu_{\text{obs}}(z_i) - \mu_{\Lambda\text{CDM}}(z_i)$, where $\mu_{\text{obs}}(z_i)$ is the observed distance modulus for each supernova at redshift z_i. Finally, we plot $\Delta\mu(z)$ against redshift to visualize how well these models align with SNe Ia data.

7. Cosmographic Parameters

In this section, we conduct a comparative analysis of the standard ΛCDM model, the interacting model, and the noninteracting model by examining several cosmographic parameters. Using the mean values from the MCMC analysis, we generate cosmographic plots for the deceleration parameter $q(z)$, jerk parameter $j(z)$, and snap parameter $s(z)$. The deceleration parameter $q(z)$ indicates whether cosmic expansion is accelerating ($q < 0$) or decelerating ($q > 0$), with the transition redshift z_{tr} marking the shift between these phases. The jerk parameter $j(z)$, which takes the value $j = 1$ in ΛCDM, measures changes in deceleration, while deviations suggest alternative physics. Similarly, the snap parameter $s(z)$, fixed at $s = 0$ in ΛCDM, reflects the absence of higher-order expansion effects. By analyzing these parameters, we systematically test different cosmological models and explore potential deviations

from standard cosmology. Their mathematical expressions are as follows.

Deceleration parameter:

$$q(z) = -1 + \frac{(1+z)}{H(z)}.\frac{\partial H(z)}{\partial z}.$$

Jerk parameter:

$$j(z) = q(z)(2q(z)+1) + (1+z)\frac{\partial q(z)}{\partial z}.$$

Snap parameter:

$$s(z) = \frac{j(z)-1}{3\left(q(z)-\frac{1}{2}\right)}.$$

These parameters offer valuable information for testing cosmological models and probing the underlying physics driving the expansion of the Universe.

8. $Om(z)$ Diagnostic

In this section, we use the $Om(z)$ diagnostic test (U. Alam et al. 2003, 2004; V. Sahni et al. 2003; M. Martinelli et al. 2020) to compare the cosmological behavior of the interacting and noninteracting models with the standard ΛCDM model. The $Om(z)$ diagnostic is a model-independent tool used to assess the nature of DE and its impact on the expansion of the Universe. Mathematically, it is calculated using the formula

$$Om(z) = \frac{H^2(z)/H_0^2 - 1}{(1+z)^3 - 1}.$$

Using the mean values from the MCMC analysis, we compare the $Om(z)$ profile of the ΛCDM model with the interacting and noninteracting models as a function of redshift. If $Om(z)$ increases with redshift (a positive slope), it suggests phantom-like behavior, where DE becomes more dominant as the Universe evolves. On the other hand, if $Om(z)$ decreases over time (a negative slope), it indicates quintessence-like behavior, meaning DE is less dominant and the expansion rate could slow down.

9. Statistical Metrics

To differentiate the interacting and noninteracting models from the ΛCDM model, we employed statistical measures to evaluate their performance. One key metric is the reduced chi-squared, defined as

$$\chi^2_{\rm red} = \frac{\chi^2_{\rm tot,min}}{\rm DOF},$$

where $\chi^2_{\rm tot,min}$ represents the minimum total chi-squared value, and DOF is the degrees of freedom, the number of data points minus the number of free parameters in the model. A reduced-chi-squared value close to 1 ($\chi^2_{\rm red} \approx 1$) indicates a good fit, values significantly less than 1 ($\chi^2_{\rm red} < 1$) suggest overfitting, while values much greater than 1 ($\chi^2_{\rm red} \gg 1$) imply a poor fit (R. Andrae et al. 2010). To further assess model performance, we calculated the Akaike information criterion (AIC) and the Bayesian information criterion (BIC; H. Akaike 1974; M. Tan & R. Biswas 2012; S. I. Vrieze 2012; F. Arevalo et al. 2017; M. Rezaei & M. Malekjani 2021). The AIC is given by

$$\rm AIC = \chi^2_{tot,min} + 2k,$$

and the BIC is defined as

$$\rm BIC = \chi^2_{tot,min} + k \ln N_{tot},$$

where k is the number of model parameters, and $N_{\rm tot}$ is the number of data points. Both criteria balance model fit and complexity, with lower values indicating better performance. To compare the models relative to ΛCDM, we computed the differences:

$$\Delta\rm AIC = AIC_{Interacting/Noninteracting} - AIC_{\Lambda CDM},$$
$$\Delta\rm BIC = BIC_{Interacting/Noninteracting} - BIC_{\Lambda CDM}.$$

According to Jeffreys' scale (H. Jeffreys 1998), $|\Delta\rm AIC| \leqslant 2$ implies the models are comparable, while $|\Delta\rm AIC| \geqslant 4$ disfavors the model with the higher AIC. For BIC, $|\Delta\rm BIC| \leqslant 2$ suggests weak evidence against the model, $2 < |\Delta\rm BIC| \leqslant 6$ indicates strong evidence, and $|\Delta\rm BIC| > 6$ shows very strong disfavor. Negative ΔAIC or ΔBIC values favor the interacting or noninteracting models over ΛCDM. Consequently the p-value was calculated as

$$p = 1 - F_{\chi^2_{\rm tot,min}}(\chi|\nu),$$

where $F_{\chi^2_{\rm tot,min}}(\chi|\nu)$ is the cumulative distribution function of the chi-squared distribution, and ν is the degrees of freedom. The p-value represents the probability of obtaining results as extreme as those observed under the null hypothesis. A p-value less than 0.05 ($p < 0.05$) indicates statistical significance, providing strong evidence against the null hypothesis.

10. Results

MCMC Results. Figures 1 and 2 display the confidence contours at the 1σ and 2σ levels for the interacting and noninteracting models, respectively. Table 1 shows the mean values along with 95% (2σ) credible intervals of the each parameters for the ΛCDM, interacting, and noninteracting models. In the ΛCDM model, the estimated value of H_0 is in close agreement with the predictions from Planck Collaboration et al. (2020) and DESI-IV. Similarly, the values of Ω_{m0} and r_d also show strong consistency with the results from Planck Collaboration et al. (2020). In the case of the interacting and noninteracting models, the values for H_0 and r_d are consistent with those predicted by Planck Collaboration et al. (2020). In the noninteracting model, $\Omega_{\rm dm_0}$ is 0.2704, and $\Omega_{\rm de_0}$ is 0.6845. However, in the interacting model, due to the interaction parameter γ, $\Omega_{\rm dm_0}$ decreases to 0.2417, and $\Omega_{\rm de_0}$ increases to 0.7132. This suggests that DM is converting into DE, which is supported by the negative value of γ, indicating the interaction between the two. The overall composition of DM and DE can be seen in Figure 3.

Hubble Parameter, Hubble Difference, Distance Modulus and Distance Modulus Difference Results. Figure 4 shows evolution of the Hubble parameters, where all three models align closely at $z < 1.5$. At higher redshifts ($z > 1.5$), a small but noticeable deviation appears, although the difference remains minimal. Figure 5 illustrates the evolution of the Hubble difference between the ΛCDM, interacting, and noninteracting models. It can be observed that the differences between these models become negligible at $z < 1.5$, but at

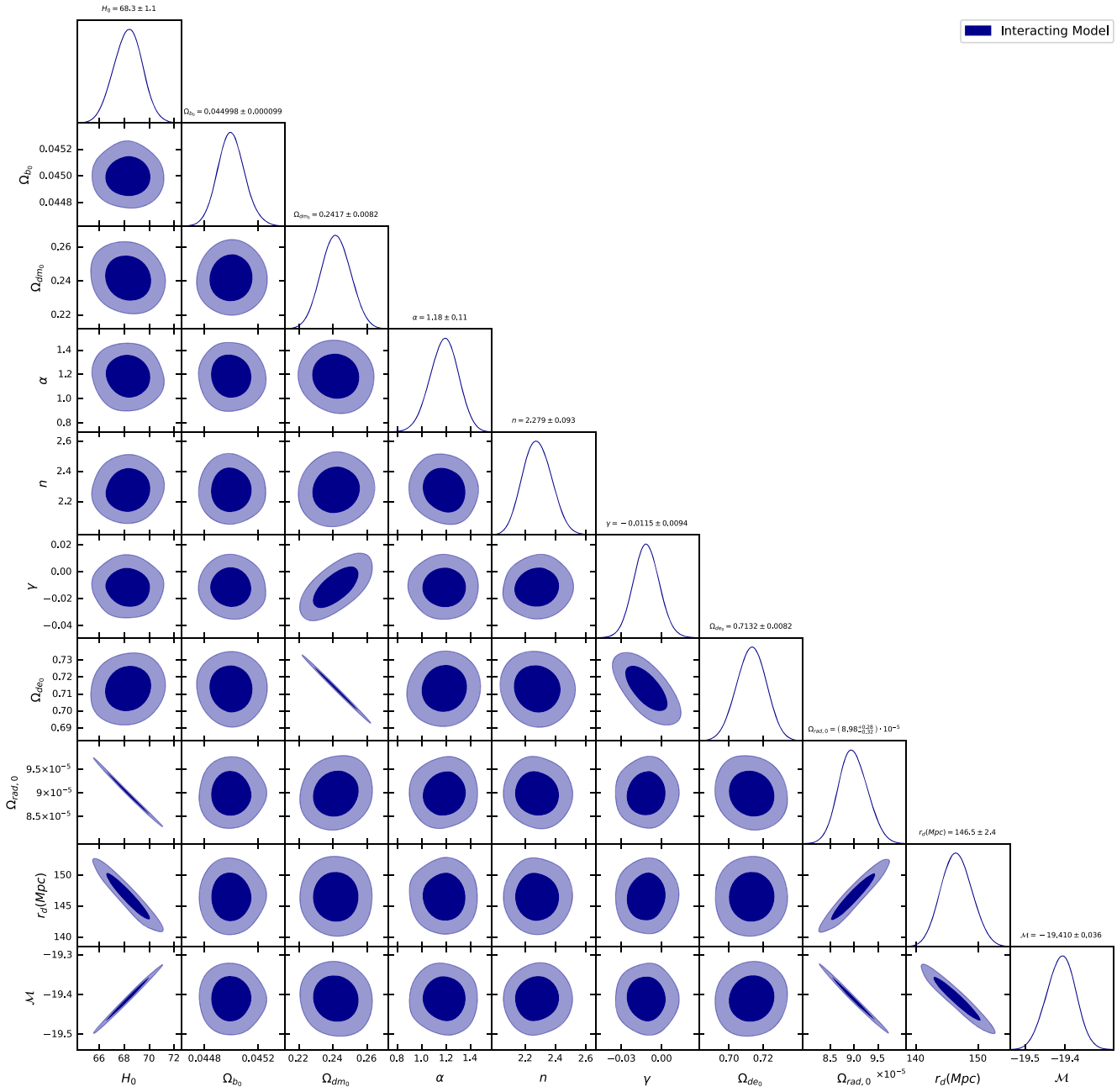

Figure 1. The confidence contours at the 68% (1σ) and 95% (2σ) levels based on constraints for the interacting model.

$z > 1.5$, a slight deviation is evident, though still minimal. Figure 6 illustrates the evolution of the distance modulus for the ΛCDM, interacting, and noninteracting models. It can be observed that all three models closely align with each other and with the SNe Ia data. Additionally, the insets in the corresponding plots highlight that the interacting model is more closely aligned with the ΛCDM model, followed by the noninteracting model, which is nearly indistinguishable to the naked eye. Figure 7 shows the residuals of the distance modulus. The differences between the ΛCDM model and the interacting and noninteracting models are very small. An inset panel is included to emphasize this, showing that the differences are almost negligible. This suggests that both the interacting and noninteracting models closely match the ΛCDM model and current data set.

Cosmographic Results. Figure 8 displays the evolution of the deceleration parameter, $q(z)$, as a function of redshift for the interacting, noninteracting, and ΛCDM models. Initially, all three models predict a deceleration parameter value around $q(z) = 0.445$, indicating a decelerating phase in the early stages of cosmic evolution. At present ($z = 0$), the ΛCDM model predicts $q(0) = -0.545$, the interacting model predicts $q(0) = -0.523$, and the noninteracting model predicts $q(0) = -0.562$, confirming that the Universe is currently in an accelerated expansion phase in all three models. The transition redshift $z_{\rm tr}$, marking the point at which the Universe transitions from deceleration to acceleration, varies slightly between the models. The ΛCDM model predicts $z_{\rm tr} = 0.671$, indicating the transition occurs earlier compared to the other models. The interacting model predicts $z_{\rm tr} = 0.616$, suggesting that

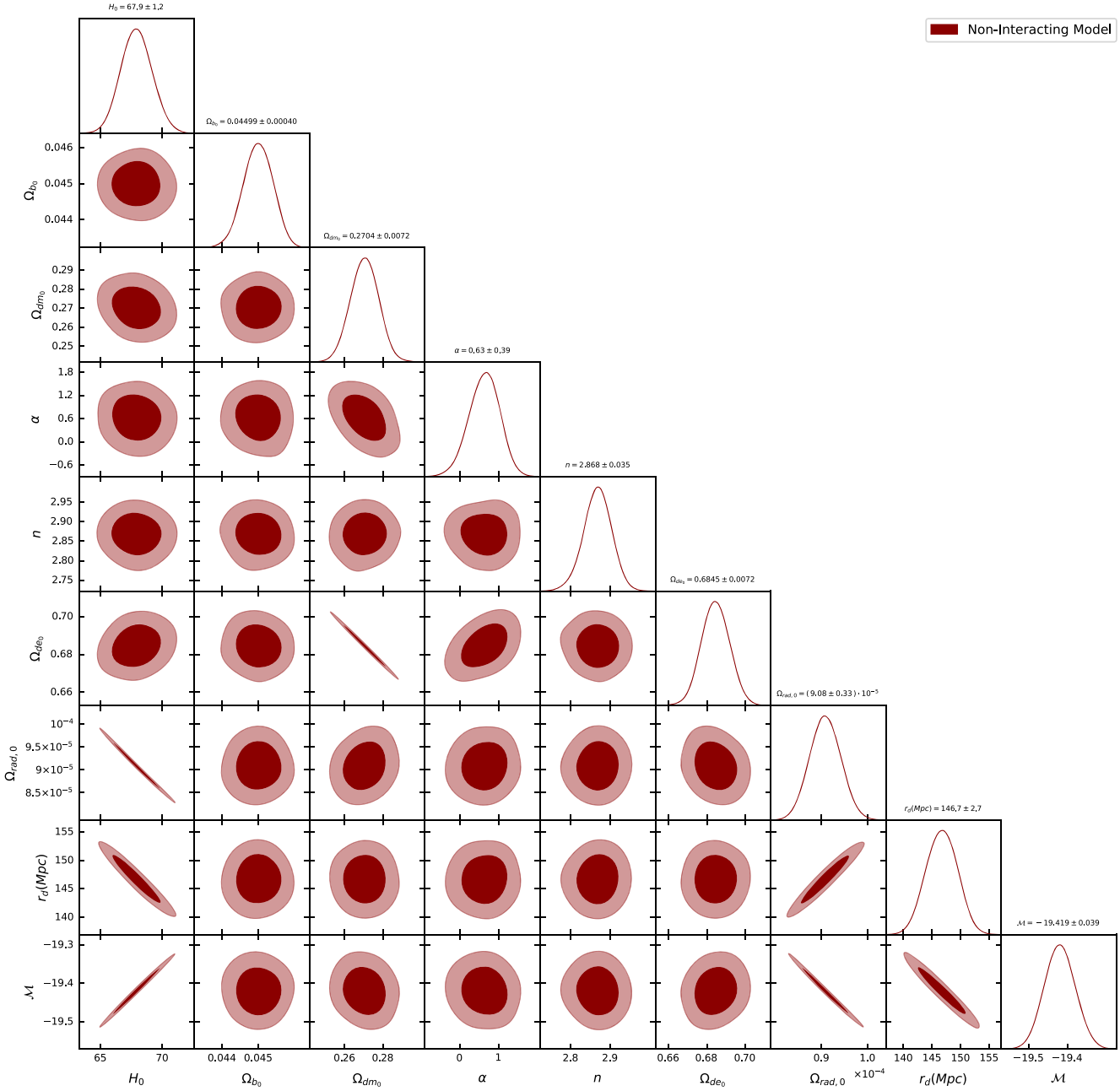

Figure 2. The confidence contours at the 68% (1σ) and 95% (2σ) levels based on constraints for the noninteracting model.

interactions between DM and DE lead to a slightly later onset of cosmic acceleration. The noninteracting model predicts $z_{\rm tr} = 0.598$, indicating the latest transition among the three models. Figure 9 shows the evolution of the jerk parameter $j(z)$. In the ΛCDM scenario, the value of the jerk parameter $j(z)$ remains constant at $j(z) = 1$ throughout the cosmic evolution. In contrast, both the interacting and noninteracting models also initially predict $j(z) = 1$, aligning with the ΛCDM model in the early stages of cosmic evolution. However, as the Universe evolves, these two models exhibit distinct dynamical behaviors due to the underlying interactions or phase transition mechanisms. Despite these differences during evolution, both the interacting and noninteracting models converge to the present-day value of $j(0) = 1$, consistent with the ΛCDM prediction at $z = 0$. Figure 10 shows the evolution of the snap parameter $s(z)$. In the ΛCDM model, $s(z)$ remains constant at $s(z) = 0$ throughout the entire cosmic evolution. In contrast, the noninteracting and interacting models show distinct initial behaviors. Initially, the noninteracting model predicts $s(z) = 0.08$, whereas the interacting model predicts $s(z) = -0.08$. These initial differences signify variations in the early Universe dynamics driven by the respective assumptions of the two models. As the Universe evolves, these two models exhibit different dynamical behaviors, reflecting their distinct physics. However, at present ($z = 0$), both the noninteracting and interacting models converge to $s(0) = 0$, aligning with the ΛCDM model's prediction for the current epoch.

Om(z) *Diagnostic Results*. Figure 11 illustrates the evolution of the $Om(z)$ diagnostic as a function of redshift. In both interacting and noninteracting models, $Om(z)$ displays a monotonic increase with increasing redshift. This behavior is characteristic of a phantom-like evolution.

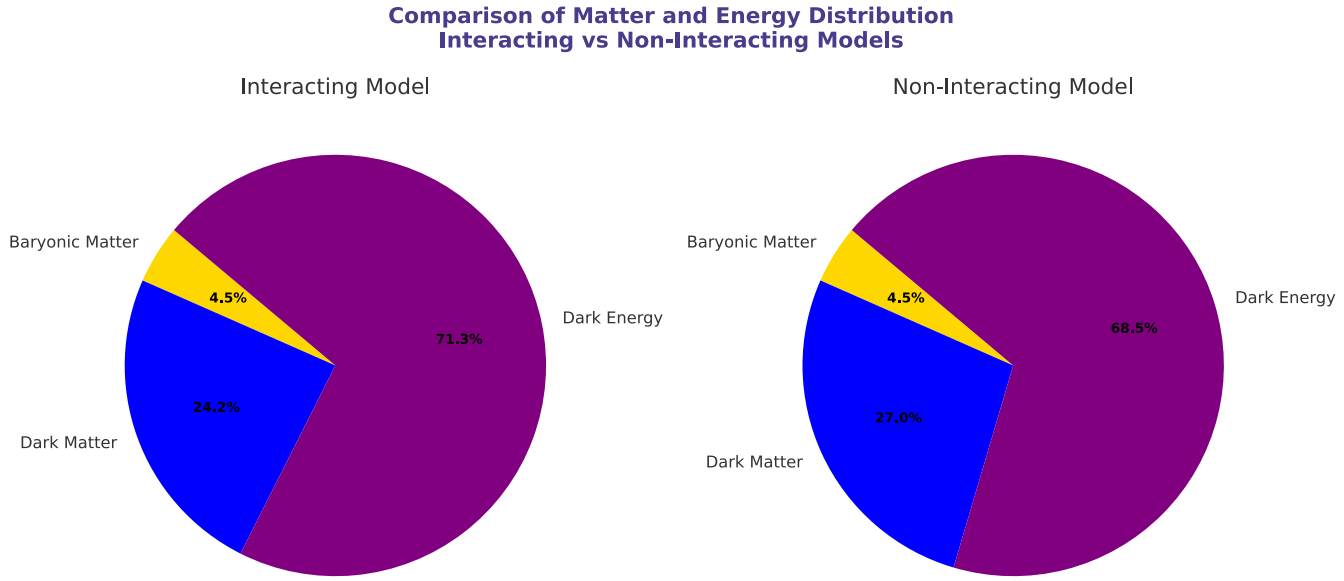

Figure 3. Comparison of matter and energy distribution: interacting vs. noninteracting cosmological models.

Table 1
Mean Values, along with 95% (2σ) Credible Intervals, and Prior Ranges for Parameters of the ΛCDM, Interacting, and Noninteracting Models

Models	Parameter	Prior	Joint
ΛCDM Model	H_0	[50., 100.]	68.1 ± 1.2
	Ω_{m0}	[0., 1.]	0.3195 ± 0.0075
	$\Omega_{\Lambda 0}$	[0., 1.]	0.6805 ± 0.0075
	r_d (Mpc)	[100., 300.]	146.5 ± 2.4
	$\mathcal{M}$	[−20., −18.]	-19.413 ± 0.037
Interacting Model	H_0	[50., 100.]	68.3 ± 1.1
	Ω_{b0}	[0., 0.1]	0.044998 ± 0.000099
	$\Omega_{\rm dm0}$	[0., 1.]	0.2417 ± 0.0082
	α	[0., 2.]	1.18 ± 0.11
	n	[1., 3.]	2.279 ± 0.093
	γ	[−0.1, 0.1]	-0.0115 ± 0.0094
	$\Omega_{\rm de0}$	[0., 1.]	0.7132 ± 0.0082
	$\Omega_{\rm rad,0}$	[0., 0.1]	$(8.98 \pm 0.28) \times 10^{-5}$
	r_d (Mpc)	[100., 300.]	146.5 ± 2.4
	$\mathcal{M}$	[−20., −18.]	-19.410 ± 0.036
Noninteracting Model	H_0	[50., 100.]	67.9 ± 1.2
	Ω_{b0}	[0., 0.1]	0.04499 ± 0.00040
	$\Omega_{\rm dm0}$	[0., 1.]	0.2704 ± 0.0072
	α	[0., 1.]	0.63 ± 0.39
	n	[1., 3.]	2.868 ± 0.035
	$\Omega_{\rm de0}$	[0., 1.]	0.6845 ± 0.0072
	$\Omega_{\rm rad,0}$	[0., 0.1]	$(9.08 \pm 0.33) \times 10^{-5}$
	r_d (Mpc)	[100., 300.]	146.7 ± 2.7
	$\mathcal{M}$	[−20., −18.]	-19.419 ± 0.039

Statistical Results. Table 2 provides a detailed comparative analysis of the ΛCDM, interacting, and noninteracting models based on several statistical metrics. The ΛCDM model has a $\chi^2_{\rm tot,min}$ value of 1798.49, with 1758 data points, 4 free parameters, and 1 redundant parameter, yielding $\chi^2_{\rm red} = 1.025$. Its AIC and BIC values are 1806.49 and 1828.37, respectively, serving as the reference model for computing ΔAIC and ΔBIC. The p-value of 0.224 indicates a statistically reasonable fit to the data. The interacting model, with a $\chi^2_{\rm tot,min}$ of 1771.59,

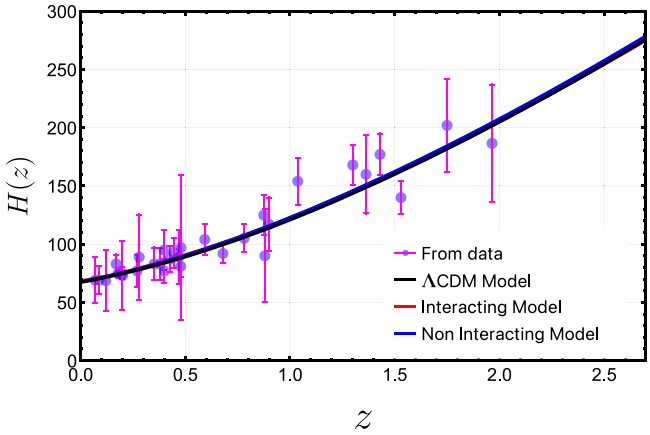

Figure 4. The evolution of the Hubble parameter as a function of redshift is presented for the ΛCDM model (black line), the interacting model (red line), and the noninteracting model (blue line). These are compared against the observational Hubble measurements, represented by purple dots with corresponding error bars shown as magenta lines.

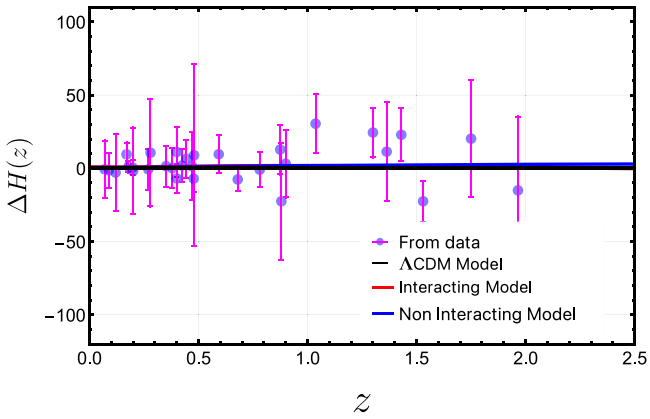

Figure 5. The evolution of the Hubble difference as a function of redshift is presented for the ΛCDM model (black line), the interacting model (red line), and the noninteracting model (blue line). These are compared against the observational Hubble measurements, represented by purple dots with corresponding error bars shown as magenta lines.

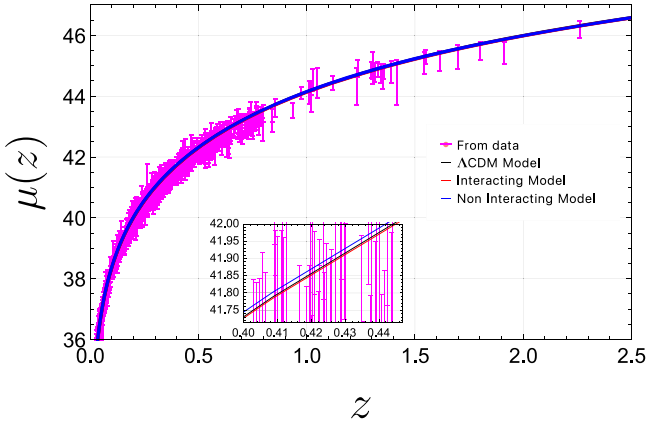

Figure 6. The evolution of the distance modulus as a function of redshift is presented for the ΛCDM model (black line), the interacting model (red line), and the noninteracting model (blue line). These are compared against the observational Hubble measurements, represented by purple dots with corresponding error bars shown as magenta lines.

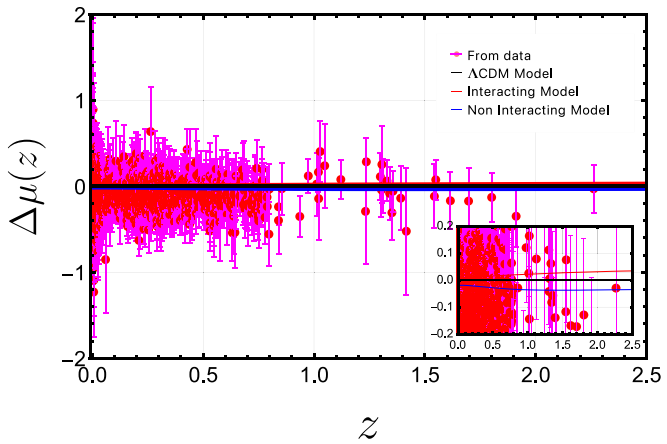

Figure 7. The evolution of the distance modulus difference as a function of redshift is presented for the ΛCDM model (black line), the interacting model (red line), and the noninteracting model (blue line). These are compared against the observational Hubble measurements, represented by purple dots with corresponding error bars shown as magenta lines.

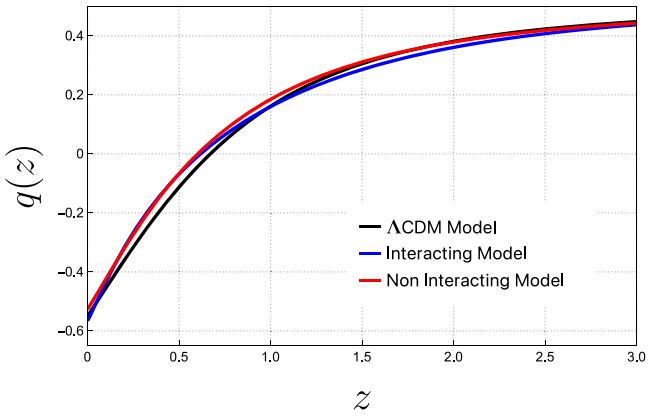

Figure 8. The evolution of deceleration parameter as a function of redshift (z).

eight free parameters, and two redundant parameters, has a slightly better reduced-chi-squared value of $\chi^2_{\rm red} = 1.012$, suggesting an improved fit compared to ΛCDM. Its AIC value of 1787.59 results in $\Delta{\rm AIC} = -18.90$, strongly favoring the interacting model over ΛCDM. However, its BIC value of

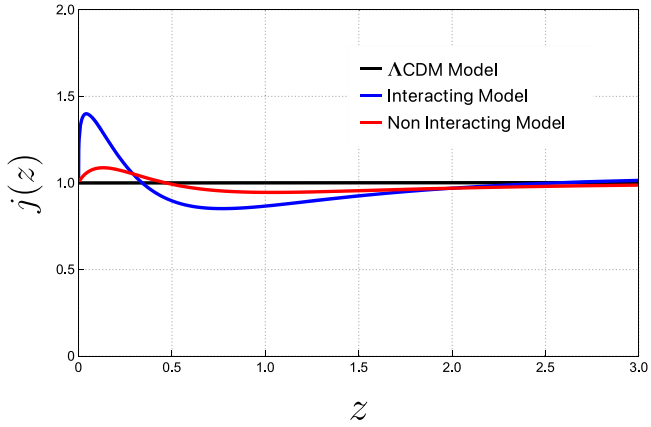

Figure 9. The evolution of jerk parameter as a function of redshift (z).

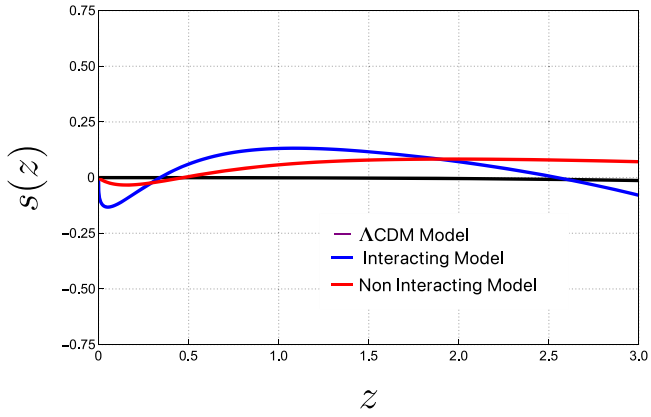

Figure 10. The evolution of snap parameter as a function of redshift (z).

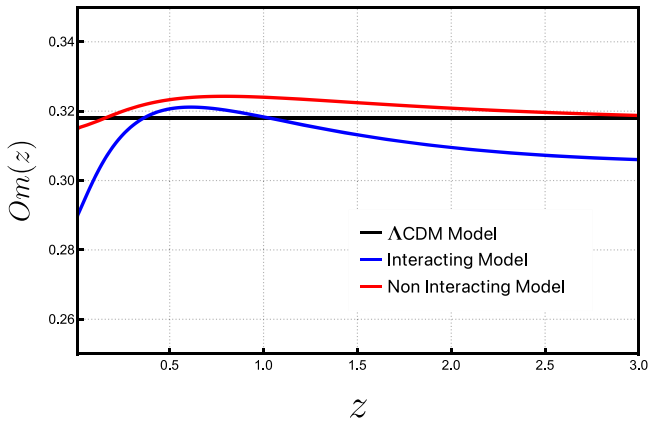

Figure 11. Evolution of the $Om(z)$ diagnostic as a function of redshift z.

1831.36 yields $\Delta{\rm BIC} = 2.98$, indicating the interacting model is weakly disfavored when penalizing for additional parameters. The p-value of 0.353 shows a good statistical fit. The noninteracting model achieves a $\chi^2_{\rm tot,min}$ of 1778.97, with seven free parameters, and two redundant parameters, resulting in $\chi^2_{\rm red} = 1.015$. Its AIC value of 1792.97 produces $\Delta{\rm AIC} = -13.51$, favoring it over ΛCDM, although less strongly than the Interacting model. Its BIC value of 1831.27 ($\Delta{\rm BIC} = 2.89$) is similar to that of ΛCDM, indicating no significant preference. The p-value of 0.315 indicates a comparable statistical fit.

Table 2
Statistical Metrics for ΛCDM, Interacting, and Noninteracting Models, including $\chi^2_{\rm tot,min}$, $\chi^2_{\rm red}$, AIC, ΔAIC, ΔBIC, and p-values

Model	$\chi^2_{\rm tot,min}$	$N_{\rm tot}$	k	$\chi^2_{\rm red}$	AIC	ΔAIC	BIC	ΔBIC	p-value
ΛCDM Model	1798.49	1758	4	1.025	1806.49	0	1828.37	0	0.224
Interacting Model	1771.59	1758	8	1.012	1787.59	−18.90	1831.36	2.98	0.353
Noninteracting Model	1778.97	1758	7	1.015	1792.97	−13.51	1831.27	2.89	0.315

11. Conclusion

Our study explores the role of interactions between DM and DE in the evolution of the Universe. By incorporating an interaction parameter into the DE model, we found evidence that DM may be converting into DE. This was reflected in the decrease of DM density ($\Omega_{\rm dm_0}$) and a corresponding increase in DE density ($\Omega_{\rm de_0}$) when comparing the interacting model to the standard ΛCDM model. The negative value of the interaction parameter (γ) supports this energy transfer, providing a new perspective on the relationship between these two dark components. From a statistical standpoint, the interacting model demonstrates a better fit to the observational data compared to ΛCDM. The AIC strongly favors the interacting model, with a ΔAIC of −18.90, indicating a more robust explanation of the data despite the additional parameters. However, when penalizing for additional parameters as in the BIC, the preference for the interacting model is weaker, though still competitive. Our cosmographic analysis revealed that the interacting model predicts a later transition from cosmic deceleration to acceleration compared to ΛCDM. This delayed transition aligns with the idea that interactions between DM and DE influence the Universe's accelerated expansion. While all models converge on present-day values for key parameters, their differences in early and late-time evolution highlight the unique physics captured by the interacting model. In conclusion, our findings suggest that the interacting model provides a more nuanced understanding of the dynamics of the dark sector. It not only fits current observational data but also offers insights into the energy transfer between DM and DE. These results emphasize the importance of considering dark-sector interactions in cosmological studies, as they could be key to understanding the Universe's accelerated expansion.

ORCID iDs

Himanshu Chaudhary https://orcid.org/0000-0002-6376-0707
Ritika Nagpal https://orcid.org/0000-0002-4669-6395
S. K. J. Pacif https://orcid.org/0000-0003-0951-414X
G. Mustafa https://orcid.org/0000-0003-1409-2009

References

Abdalla, E., Abramo, L. R., & de Souza, J. C. 2010, PhRvD, 82, 023508
Adame, A., Aguilar, J., Ahlen, S., et al. 2025, JCAP, 2025, 021
Aich, A. 2023, ARep, 67, 537
Akaike, H. 1974, ITAC, 19, 716
Alam, S., Aubert, M., Avila, S., et al. 2021, PhRvD, 103, 083533
Alam, U., Sahni, V., Deep Saini, T., & Starobinsky, A. 2003, MNRAS, 344, 1057
Alam, U., Sahni, V., Deep Saini, T., & Starobinsky, A. A. 2004, MNRAS, 354, 275
Amendola, L. 2000, PhRvD, 62, 043511
Amendola, L., Campos, G. C., & Rosenfeld, R. 2007, PhRvD, 75, 083506
Andrae, R., Schulze-Hartung, T., & Melchior, P. 2010, arXiv:1012.3754
Arevalo, F., Bacalhau, A. P., & Zimdahl, W. 2012, CQGra, 29, 235001
Arevalo, F., Cid, A., & Moya, J. 2017, EPJC, 77, 565
Ashmita, Banerjee, K., Das, P. K., et al. 2024, JCAP, 2024, 034
Astier, P., Guy, J., Regnault, N., et al. 2006, A&A, 447, 31
Baldi, M. 2011, MNRAS, 411, 1077
Bamba, K., Capozziello, S., Nojiri, S., & Odintsov, S. D. 2012, Ap&SS, 342, 155
Belli, S., Newman, A. B., & Ellis, R. S. 2019, ApJ, 874, 17
Bolotin, Y. L., Kostenko, A., Lemets, O. A., & Yerokhin, D. A. 2015, IJMPD, 24, 1530007
Brout, D., Scolnic, D., Popovic, B., et al. 2022, ApJ, 938, 110
Cai, R.-G., & Wang, A. 2005, JCAP, 2005, 002
Caldera-Cabral, G., Maartens, R., & Schaefer, B. M. 2009, JCAP, 2009, 027
Carnall, A., McLure, R., Dunlop, J., & Davé, R. 2018, MNRAS, 480, 4379
Choi, J., Conroy, C., Moustakas, J., et al. 2014, ApJ, 792, 95
Cimatti, A., Daddi, E., Renzini, A., et al. 2004, Natur, 430, 184
Citro, A., Pozzetti, L., Moresco, M., & Cimatti, A. 2016, A&A, 592, A19
Conley, A., Guy, J., Sullivan, M., et al. 2010, ApJS, 192, 1
Copeland, E. J., Sami, M., & Tsujikawa, S. 2006, IJMPD, 15, 1753
Costa, A. A., Xu, X.-D., Wang, B., Ferreira, E. G., & Abdalla, E. 2014, PhRvD, 89, 103531
Costa, F., Alcaniz, J., & Jain, D. 2012, PhRvD, 85, 107302
Di Valentino, E., Mena, O., Pan, S., et al. 2021, CQGra, 38, 153001
Estrada-Carpenter, V., Papovich, C., Momcheva, I., et al. 2018, ApJ, 870, 133
Farrar, G. R., & Peebles, P. J. E. 2004, ApJ, 604, 1
Gavela, M. B., Honorez, L. L., Mena, O., & Rigolin, S. 2010, JCAP, 2010, 044
Guo, Z.-K., Ohta, N., & Tsujikawa, S. 2007, PhRvD, 76, 023508
Handley, W., Hobson, M., & Lasenby, A. 2015, MNRAS, 450, L61
He, J.-H., Wang, B., & Abdalla, E. 2009a, PhLB, 671, 139
He, J.-H., Wang, B., & Zhang, P. 2009b, PhRvD, 80, 063530
Huchra, J., Davis, M., Latham, D., & Tonry, J. 1983, ApJS, 52, 89
Hussain, S., Arora, S., Rana, Y., Rose, B., & Wang, A. 2024, JCAP, 2024, 042
Jedamzik, K., Pogosian, L., & Zhao, G.-B. 2021, CmPhy, 4, 123
Jeffreys, H. 1998, The Theory of Probability (Oxford: Oxford Univ. Press)
Jimenez, R., & Loeb, A. 2002, ApJ, 573, 37
Jimenez, R., Verde, L., Treu, T., & Stern, D. 2003, ApJ, 593, 622
Komatsu, E., Smith, K. M., Dunkley, J., et al. 2011, ApJS, 192, 18
Lewis, A. 2019, arXiv:1910.13970
Lin, W., Chen, X., & Mack, K. J. 2021, ApJ, 920, 159
Liu, Y., Liao, S., Liu, X., et al. 2022, MNRAS, 511, 3076
Ludwick, K. J., & Sebaugh, H. 2021, MPLA, 36, 2150122
Maffei, B., De Bernardis, P., Aghanim, N., & Stever, S. 2022, Phot, 116, 38
Majerotto, E., Väliviita, J., & Maartens, R. 2009, NuPhS, 194, 260
Martinelli, M., Martins, C. J. A. P., Nesseris, S., et al. 2020, A&A, 644, A80
Micheletti, S., Abdalla, E., & Wang, B. 2009, PhRvD, 79, 123506
Mishra, K. R., Pacif, S. K. J., Kumar, R., & Bamba, K. 2023, PDU, 40, 101211
Montani, G., Carlevaro, N., Escamilla, L. A., & Di Valentino, E. 2025, PDU, 48, 101848
Moresco, M., Jimenez, R., Verde, L., Cimatti, A., & Pozzetti, L. 2020, ApJ, 898, 82
Moresco, M., Pozzetti, L., Cimatti, A., et al. 2016, JCAP, 2016, 014
Moresco, M., Verde, L., Pozzetti, L., Jimenez, R., & Cimatti, A. 2012, JCAP, 2012, 053
Nagpal, R., & Pacif, S. K. J. 2021, EPJP, 136, 875
Nazari Pooya, N. 2024, PhRvD, 110, 043510
Nunes, R. C., & Vagnozzi, S. 2021, MNRAS, 505, 5427
Onodera, M., Carollo, C. M., Renzini, A., et al. 2015, ApJ, 808, 161
Pacifici, C., Kassin, S. A., Weiner, B. J., et al. 2016, ApJ, 832, 79
Pavón, D., & Wang, B. 2009, GReGr, 41, 1
Penzias, A. A., & Wilson, R. W. 1965, ApJ, 142, 419
Perlmutter, S., Aldering, G., Goldhaber, G., et al. 1999, ApJ, 517, 565
Planck Collaboration, Aghanim, N., Akrami, Y., et al. 2020, A&A, 641, A6
Pogosian, L., Zhao, G.-B., & Jedamzik, K. 2020, ApJL, 904, L17
Pogosian, L., Zhao, G.-B., & Jedamzik, K. 2024, ApJL, 973, L13
Pozzetti, L., Bolzonella, M., Zucca, E., et al. 2010, A&A, 523, A13
Ratsimbazafy, A., Loubser, S., Crawford, S., et al. 2017, MNRAS, 467, 3239
Rezaei, M., & Malekjani, M. 2021, EPJP, 136, 219

Riess, A. G., Casertano, S., Yuan, W., Macri, L. M., & Scolnic, D. 2019, ApJ, 876, 85
Riess, A. G., Filippenko, A. V., Challis, P., et al. 1998, AJ, 116, 1009
Rodriguez-Benites, C., Gonzalez-Espinoza, M., Otalora, G., & Alva-Morales, M. 2024, EPJC, 84, 276
Sahni, V., Saini, T. D., Starobinsky, A. A., & Alam, U. 2003, JETPL, 77, 201
Salvatelli, V., Marchini, A., Lopez-Honorez, L., & Mena, O. 2013, PhRvD, 88, 023531
Salvatelli, V., Said, N., Bruni, M., Melchiorri, A., & Wands, D. 2014, PhRvL, 113, 181301
Saraf, C. S., & Bielewicz, P. 2024, A&A, 687, A150
Simon, J., Verde, L., & Jimenez, R. 2005, PhRvD, 71, 123001
Singh, J., & Nagpal, R. 2024, InJPh, 98, 2609
Skilling, J. 2006, Bayesian Anal., 1, 833
Steinhardt, P. J., Wang, L., & Zlatev, I. 1999, PhRvD, 59, 123504
Stern, D., Jimenez, R., Verde, L., Kamionkowski, M., & Stanford, S. A. 2010, JCAP, 2010, 008
Tan, M., & Biswas, R. 2012, MNRAS, 419, 3292
Thomas, D., Maraston, C., Schawinski, K., Sarzi, M., & Silk, J. 2010, MNRAS, 404, 1775
Treu, T., Ellis, R. S., Liao, T. X., et al. 2005, ApJ, 633, 174
Vagnozzi, S. 2023, Univ, 9, 393
Vagnozzi, S., Loeb, A., & Moresco, M. 2021, ApJ, 908, 84
Verde, L., Treu, T., & Riess, A. G. 2019, NatAs, 3, 891
Vrieze, S. I. 2012, Psychol. Methods, 17, 228
Wang, B., Abdalla, E., Atrio-Barandela, F., & Pavon, D. 2016, RPPh, 79, 096901
Wang, D., & Meng, X.-H. 2017, PhRvD, 96, 103516
Weinberg, S. 1989, RvMP, 61, 1
Wetterich, C. 1995, A&A, 301, 321
Wong, K. C., Suyu, S. H., Chen, G. C., et al. 2020, MNRAS, 498, 1420
Yang, W., Li, H., Wu, Y., & Lu, J. 2016, JCAP, 2016, 007
Yang, W., Pan, S., Di Valentino, E., et al. 2018, JCAP, 2018, 019
Zhang, C., Zhang, H., Yuan, S., et al. 2014, RAA, 14, 1221
Zimdahl, W. 2012, Models of Interacting Dark Energy in AIP Conf. Proc. 1471, I COSMOSUL: Cosmology and Gravitation in the Southern Cone, ed. J. Alcaniz et al. (Melville, NY: AIP)